

Towards a Refined Understanding of Non-holomorphic Soft SUSY-Breaking Effects on the Higgs Boson Mass Spectra

M. REHMAN^{1*} AND S. HEINEMEYER^{2†}

¹*Department of Physics, Comsats University Islamabad, 44000 Islamabad, Pakistan*

²*Instituto de Física Teórica, (UAM/CSIC), Universidad Autónoma de Madrid, Cantoblanco, 28049 Madrid, Spain*

Abstract

We study the impact of the non-holomorphic (NH) soft supersymmetry-breaking terms $T'_{33}{}^D$ and μ' , which introduce additional SUSY-breaking effects beyond the holomorphic structure of the superpotential, on the Higgs boson mass spectrum in the NH Minimal Supersymmetric Standard Model (NHSSM). The term $T'_{33}{}^D$ modifies the scalar bottom-quark mass matrix and Higgs couplings, while μ' affects the mass matrices of charginos and neutralinos. In our analysis, we incorporate constraints from charge- and color-breaking (CCB) minima where we find that a portion of the parameter space is excluded by these constraints. Focusing on the allowed parameter space, the NH contributions to the light \mathcal{CP} -even Higgs boson mass, M_h , from μ' and $T'_{33}{}^D$ can reach up to 1.4 GeV and 90 MeV, respectively. For the heavy \mathcal{CP} -even Higgs boson mass, M_H , and the charged Higgs boson mass, M_{H^\pm} , these contributions can be substantially larger in certain regions of the parameter space, reaching up to 44 GeV for M_H and 42 GeV for M_{H^\pm} due to μ' , and up to 60 GeV due to $T'_{33}{}^D$ for both M_H and M_{H^\pm} . These corrections are significantly larger than the expected future experimental precision for Higgs boson masses and should therefore be considered in precision analyses for future experiments.

*email: m.rehman@comsats.edu.pk

†email: Sven.Heinemeyer@cern.ch

1 Introduction

The Minimal Supersymmetric Standard Model (MSSM) [1–6] is an important theoretical framework for studying and exploring physics beyond the Standard Model (SM). The introduction of supersymmetry (SUSY) in the SM helps address some fundamental questions in particle physics, such as the hierarchy problem and the nature of dark matter. The MSSM provides natural candidates for dark matter in the form of the lightest supersymmetric particle (LSP), which is typically stable and weakly interacting. The MSSM requires two Higgs doublets, leading to additional Higgs bosons compared to the SM, including two charged Higgs bosons H^\pm , one \mathcal{CP} -odd Higgs boson A , and two neutral \mathcal{CP} -even Higgs bosons h and H . The ratio of the vacuum expectation values of these doublets is defined by the parameter $\tan\beta := v_2/v_1$, where typically values ranging from 1 to 50 are assumed. These additional Higgs bosons offer distinctive signatures that can be explored at particle colliders.

Despite extensive searches, the large hadron collider (LHC) has not yet observed any direct evidence of SUSY particles nor for any other beyond the SM (BSM) particle. The LHC experiments, particularly ATLAS and CMS, have been able to set increasingly stringent lower limits on the masses of SUSY particles. These mass bounds have ruled out certain regions of parameter space and have put pressure on some traditional MSSM scenarios. The hierarchy problem, which pertains to the fine-tuning required in the Higgs boson mass, motivated the introduction of SUSY. However, the absence of sparticles detection and the lack of significant deviations in Higgs boson properties from the SM [7] have led researchers to reconsider the naturalness argument for SUSY or to look for interactions beyond to the MSSM to explain the LHC results.

The inclusion of non-holomorphic (NH) terms allows for additional interactions and couplings in the theory [8, 9], which can have various implications for the particle spectrum, phenomenology, and experimental observables [10–18]. This extended model is known as the non-holomorphic supersymmetric standard model (NHSSM). Previous studies [19–24], have examined the effects of these NH terms, particularly in the context of the Higgs boson sector. A more recent work [25] investigated the impact of NH soft SUSY-breaking (SSB) terms on the mass of the lightest \mathcal{CP} -even Higgs boson M_h . They specifically considered the effects of these terms on the scalar top masses, which influence the left-right mixing parameter X_t . However, as discussed in Ref. [26], it is important to note that changes in the holomorphic SSB terms, specifically the trilinear Higgs-stop coupling T_{33}^U , can emulate the observed effects attributed to the NH terms. For a given value of T_{33}^U , the NH trilinear coupling of scalar top quark, the coupling T_{33}^U can be adjusted to yield the same scalar top mass. Consequently, an observed scalar top mass spectrum corresponds to a continuous range of combinations of T_{33}^U and $T_{33}^{\prime U}$ while keeping other SSB parameters and the Higgs mixing parameter μ fixed. Therefore, an analysis that solely varies $T_{33}^{\prime U}$, leading to shifts in the scalar top masses, can not be considered realistic.

Since the NH SSB terms also affect the couplings of the Higgs bosons to the scalar fermions, it is crucial to consider all potential effects simultaneously to accurately determine the genuine impact of the NH terms. This comprehensive approach is necessary to fully understand the implications of NH effects within the NHSSM. In our previous analysis [26], we investigated the impact of the parameter T_{33}^U on the masses of the Higgs bosons while ensuring that no effects on the scalar top masses and mixings arise. The influence of $T_{33}^{\prime U}$

on the mass of the lightest \mathcal{CP} -even Higgs boson M_h was found to be relatively small, in contrast to the claim in Ref. [25], with deviations only reaching a few MeV. However, the effects of T_{33}^U on the heavy \mathcal{CP} -even Higgs boson mass M_H and the charged Higgs boson mass M_{H^\pm} were significant, leading to deviations of several GeV. In the mass matrix of the scalar top sector, the coupling T_{33}^U is divided by the parameter $\tan\beta$, resulting in relatively minor effects [26]. However, in the scalar bottom sector, the NH trilinear coupling T_{33}^D is multiplied by $\tan\beta$, possibly enhancing its effect on the Higgs boson masses, particularly M_h . Additionally, the NH parameter μ' , which appears in the neutralino and chargino mass matrices, can have important implications for the Higgs boson phenomenology, particularly when considering constraints related to dark matter and low fine-tuning issue [11].

In this study, we analyze the impact of NH SSB terms, namely T_{33}^D and μ' , on the mass spectra of the Higgs bosons complementing our analysis in Ref. [26], where we focused on T_{33}^U contributions. We calculate the corresponding one-loop corrections to the NHSSM Higgs-boson masses in the Feynman diagrammatic approach. The analysis of the effects on the Higgs-boson masses was performed with the help of **SPheno** [27] source code specifically designed for the NHSSM. This source code was obtained through the Mathematica package **SARAH** [28–32], which provides a framework for generating the necessary model files and calculations for particle physics phenomenology. In the numerical analysis, similar to our approach in Ref. [26], we ensured that the physical masses of the particles entering the loop contributions are either fixed, or vary only slightly, below possible future experimental precisions. This is crucial for a realistic set-up.

The structure of the paper is outlined as follows: initially, we describe the key characteristics of the NHSSM in Sect. 2. The computational framework is discussed in Sect. 3 and our numerical findings are presented in Sect. 4. Lastly, our conclusions are summarized in Sect. 5.

2 Model set-up

The superpotential within the MSSM is required to be holomorphic, leading to the parametrization of the SSB sector primarily with holomorphic operators. Nevertheless, it is possible to extend the MSSM by incorporating R-Parity violating and/or NH terms in the SSB sector [8, 9, 15]. In its simplest form, the SSB sector of the MSSM can include the following terms:

$$-\mathcal{L}_{\text{soft}}^{\text{NH}} = T_{ij}'^D h_2 \tilde{d}_{Ri}^* \tilde{q}_{Lj} + T_{ij}'^U h_1 \tilde{u}_{Ri}^* \tilde{q}_{Lj} + T_{ij}'^E h_2 \tilde{e}_{Ri}^* \tilde{l}_{Lj} + \mu' \tilde{h}_1 \tilde{h}_2 \quad (1)$$

Here, \tilde{q}_{Li} (\tilde{l}_{Li}) are the left-handed squark (slepton) doublet fields while \tilde{u}_{Ri} , \tilde{d}_{Ri} and \tilde{e}_{Ri} are the right-handed up-type squark, down-type squark and charged slepton singlet fields respectively with $i, j = 1, 2, 3$ representing the generation index. The h_1 , h_2 represent two Higgs doublets and \tilde{h}_1 and \tilde{h}_2 are the fermionic components (Higgsinos) of the down-type and up-type Higgs superfields, respectively. The μ' represents the NH higgsino mass term. The $T_{ij}'^U = Y_{ij}^U A_{ij}'^U$, $T_{ij}'^D = Y_{ij}^D A_{ij}'^D$, and $T_{ij}'^E = Y_{ij}^E A_{ij}'^E$ denote the NH trilinear coupling matrices for up-type squarks, down-type squarks, and charged sleptons, respectively with Y_{ij} representing the corresponding Yukawa coupling. It's important to note that these terms are not necessarily related to the holomorphic trilinear soft terms. One approach is to

consider a scenario where these non-holomorphic trilinear terms are assumed to be equal to the holomorphic trilinear couplings as a "boundary condition" at the Grand Unified Theory (GUT) scale, especially in models like the Constrained MSSM. However, it's essential to acknowledge that due to renormalization group equation running effects, the NH trilinear terms will evolve differently, resulting in completely different values from the holomorphic ones, as discussed in Ref. [24]. Therefore, it is reasonable to treat the NH trilinear terms as independent quantities, although they are expected to be of similar magnitudes to the usual trilinear couplings. This approach is meaningful when comparing predictions of the NHSSM with experimental results.

In the presence of the NH trilinear terms, the down-type squarks mass matrix can be written as

$$M_{\tilde{D}}^2 = \begin{pmatrix} m_{\tilde{D}_{LL}}^2 & m_{\tilde{D}_{LR}}^2 \\ m_{\tilde{D}_{LR}}^{2\dagger} & m_{\tilde{D}_{RR}}^2 \end{pmatrix} \quad (2)$$

with

$$\begin{aligned} m_{\tilde{D}_{LL}}^2 &= m_{\tilde{Q}}^2 + M_Z^2 \cos 2\beta \left(I_3^f - Q_f s_W^2 \right) + m_d^2 \\ m_{\tilde{D}_{RR}}^2 &= m_{\tilde{D}}^2 + M_Z^2 \cos 2\beta Q_f s_W^2 + m_d^2 \\ m_{\tilde{D}_{LRii}}^2 &= \frac{v_1}{\sqrt{2}} \left(T_{ii}^D - (\mu Y_{ii}^D + T_{ii}'^D) \tan \beta \right). \end{aligned} \quad (3)$$

Here, I_3^f represents the weak isospin of fermions, Q_f stands for the electromagnetic charge, and m_d denotes the mass of the SM down-type quarks whereas $m_{\tilde{Q}}$, and $m_{\tilde{D}}$ correspond to the masses of the left-handed squark doublet and right-handed down-type squark singlet. M_Z and M_W correspond to the masses of the Z and W bosons, while s_W is defined as the square root of $1 - c_W^2$, where $c_W = M_W/M_Z$ and T_{ii}^D represent the holomorphic trilinear couplings corresponding to down-type squarks, while μ denotes the holomorphic Higgsino mass parameter. It should be noted that because of the different combination of fields, the NH trilinear couplings $T_{ii}'^D$ receive the additional factors of $\tan \beta$. The NH higgsino mass parameter μ' mentioned in Eq. (1) modifies the neutralino and chargino mass matrices given by

$$\mathbf{Y} = \begin{pmatrix} M_1 & 0 & -M_Z s_w \cos \beta & M_Z s_w \sin \beta \\ 0 & M_2 & M_Z c_w \cos \beta & -M_Z c_w \sin \beta \\ -M_Z s_w \cos \beta & M_Z c_w \cos \beta & 0 & -(\mu + \mu') \\ M_Z s_w \sin \beta & -M_Z c_w \sin \beta & -(\mu + \mu') & 0 \end{pmatrix}, \quad (4)$$

$$\mathbf{X} = \begin{pmatrix} M_2 & \sqrt{2} M_W \sin \beta \\ \sqrt{2} M_W \cos \beta & (\mu + \mu') \end{pmatrix}. \quad (5)$$

As discussed before, the the NH trilinear terms also modify the Higgs-sfermion-sfermion couplings. Here we show the couplings of the lightest Higgs boson h to the down-type squarks.

$$C(h, \tilde{d}_i^s, \tilde{d}_j^t) = \frac{-ie\delta_{ij}}{6M_W c_W s_W c_\beta} \left[3c_W m_{d_i} \left\{ s_\alpha \frac{T_{ii}^D}{Y_{ii}^D} + \left(\mu + \frac{T_{ii}'^D}{Y_{ii}^D} \right) c_\alpha \right\} U_{s,1}^{\tilde{d},i} U_{t,2}^{\tilde{d},i} \right]$$

$$\begin{aligned}
& + \{6s_\alpha c_W m_{d_i}^2 - M_W M_Z s_{\alpha+\beta} c_\beta (3 - 2s_W^2)\} U_{s,1}^{\tilde{d},i} U_{t,1}^{\tilde{d},i} \\
& + \{6s_\alpha c_W m_{d_i}^2 - 2M_W M_Z s_{\alpha+\beta} c_\beta s_W^2\} U_{s,2}^{\tilde{d},i} U_{t,2}^{\tilde{d},i} \\
& + 3c_W m_{d_i} \left\{ s_\alpha \frac{T_{ii}^D}{Y_{ii}^D} + \left(\mu + \frac{T_{ii}^{'D}}{Y_{ii}^{'D}} \right) c_\alpha \right\} U_{s,2}^{\tilde{d},i} U_{t,1}^{\tilde{d},i} \Big]
\end{aligned} \tag{6}$$

The coupling of the charged Higgs boson H^- to up-type and down-type squarks is given by

$$\begin{aligned}
C(H^-, \tilde{u}_i^s, \tilde{d}_j^t) = & \frac{ieV_{ij}^{\text{CKM}}}{2M_W s_W s_\beta} \left[m_{u_i} U_{s,2}^{\tilde{u},i} U_{t,1}^{\tilde{d},j} \left\{ \frac{T_{ii}^U}{Y_{ii}^U} + \left(\mu + \frac{T_{ii}^{'U}}{Y_{ii}^{'U}} \right) t_\beta \right\} \right. \\
& + m_{u_i} m_{d_j} U_{s,2}^{\tilde{u},i} U_{t,2}^{\tilde{d},j} (1 + t_\beta^2) + U_{s,1}^{\tilde{u},i} U_{t,2}^{\tilde{d},j} m_{d_j} t_\beta \left\{ \frac{T_{ii}^D}{Y_{ii}^D} t_\beta + \left(\mu + \frac{T_{ii}^{'D}}{Y_{ii}^{'D}} \right) \right\} \\
& \left. + U_{s,1}^{\tilde{u},i} U_{t,1}^{\tilde{d},j} \{ m_{u_i}^2 - t_\beta (M_W^2 s_{2\beta} - m_{d_j}^2) t_\beta \} \right]
\end{aligned} \tag{7}$$

Here i, j are the generation indices (we assume flavor conservation throughout the paper), $U_{s,s'}^{\tilde{u},i}$ ($U_{t,t'}^{\tilde{d},j}$) is the 2×2 rotation matrix for up-type (down-type) squarks that diagonalizes the scalar top (scalar bottom) mass matrix, and we use the shorthand notation s_x, c_x, t_x for $\sin x, \cos x, \tan x$, respectively, where α is the \mathcal{CP} -even Higgs mixing angle. The couplings of the \mathcal{CP} -even heavy Higgs boson H to the down-type squarks can be obtained by replacing $c_\alpha \rightarrow s_\alpha, s_\alpha \rightarrow -c_\alpha$ and $s_{\alpha+\beta} \rightarrow -c_{\alpha+\beta}$ in Eq. (6). It is interesting to observe that the $T_{ii}^{'D}$ enter differently into the scalar bottom masses and into the trilinear Higgs-scalar bottom couplings. In the mass matrix, it appears with a factor of $\tan \beta$, whereas the holomorphic trilinear term does not include this factor. Similarly, in the couplings, $T_{ii}^{'D}$ is multiplied by c_α , while the trilinear term is multiplied by s_α . This will be crucial for our numerical analysis, see the discussion in Sect. 4.

3 Higher order corrections in the NHSSM Higgs sector

3.1 Tree-level structure and higher-order corrections

The MSSM (and thus the NHSSM) Higgs-boson sector consist of two Higgs doublets and predicts the existence of five physical Higgs bosons, the light and heavy \mathcal{CP} -even h and H , the \mathcal{CP} -odd A , and a pair of charged Higgs bosons, H^\pm , where we assume \mathcal{CP} conservation throughout the paper. At the tree-level the Higgs sector is described with the help of two parameters: the mass of the A boson, M_A , and $\tan \beta = v_2/v_1$, the ratio of the two vacuum expectation values. The tree-level relations and in particular the tree-level masses receive large higher-order corrections, see, e.g., Refs. [33, 34] and references therein.

The lightest MSSM Higgs boson, with mass M_h , can be interpreted as the new state discovered at the LHC around ~ 125 GeV [35]. The present experimental uncertainty at the LHC for M_h , is about [36],

$$\delta M_h^{\text{exp, today}} \sim 110 \text{ MeV} . \tag{8}$$

This can possibly be reduced to the level of

$$\delta M_h^{\text{exp, future}} \lesssim 20 \text{ MeV} \tag{9}$$

at HL-LHC [37] and future e^+e^- colliders (where we take ILC [38, 39] numbers as concrete example). Similarly, for the masses of the heavy neutral Higgs M_H , an uncertainty at the 1% level could be expected at the LHC [40].

At the tree-level, the masses of the \mathcal{CP} -even Higgs bosons are given by

$$m_{(H,h),\text{tree}}^2 = \frac{1}{2} \left[M_A^2 + M_Z^2 \pm \sqrt{(M_A^2 + M_Z^2)^2 - 4M_A^2 M_Z^2 \cos 2\beta} \right] \quad (10)$$

However, the tree-level masses, receive large higher-order corrections [33, 34]. In the Feynman diagrammatic (FD) approach employed in our current calculation¹, the higher-order corrections are included in the matrix Δ_{Higgs} given by

$$(\Delta_{\text{Higgs}})^{-1} = -i \begin{pmatrix} p^2 - m_{H,\text{tree}}^2 + \hat{\Sigma}_{HH}(p^2) & \hat{\Sigma}_{hH}(p^2) \\ \hat{\Sigma}_{hH}(p^2) & p^2 - m_{h,\text{tree}}^2 + \hat{\Sigma}_{hh}(p^2) \end{pmatrix}. \quad (11)$$

The masses of the \mathcal{CP} -even Higgs bosons are determined by finding the poles of the propagator matrix for (h, H) . Determining the poles of the matrix Δ_{Higgs} in Eq. (11) is equivalent to solving the equation

$$\left[p^2 - m_{h,\text{tree}}^2 + \hat{\Sigma}_{hh}(p^2) \right] \left[p^2 - m_{H,\text{tree}}^2 + \hat{\Sigma}_{HH}(p^2) \right] - \left[\hat{\Sigma}_{hH}(p^2) \right]^2 = 0. \quad (12)$$

Likewise, concerning the charged Higgs sector, the charged Higgs mass is deduced from the position of the pole in the charged Higgs propagator [41] which can be obtained by solving the equation

$$p^2 - m_{H^\pm,\text{tree}}^2 + \hat{\Sigma}_{H-H^+}(p^2) = 0. \quad (13)$$

The (renormalized) self-energies of the Higgs bosons as described in Eqs. (12) and 13 can be computed at the n -loop level through explicit FD calculations of the relevant loop diagrams. As previously mentioned, our focus in this study will be primarily on the one-loop corrections originating from the bottom/sbottom sector and μ' . Generic Feynman diagrams that involve NH couplings are shown in the Fig. 1. Here, we restrict our analysis to quark/squark contributions only, as these are the only sectors affected by $T_{33}'^D$ or μ' . The parameter μ' does not enter the interaction vertices but contributes solely to the chargino and neutralino mass matrices. Consequently, by fixing the combination $\mu + \mu'$ to a constant value—an approach adopted in this analysis—the neutralino and chargino sectors remain unaffected by variations in μ' .

The NH SSB parameters in the NHSSM play a crucial role in the one-loop computation of the various (renormalized) self-energies and tadpoles of the Higgs bosons. As previously discussed, these parameters impact scalar fermion masses as well as the Higgs-sfermion-sfermion coupling, as depicted in Eqs. (6)-(7), which will be particularly significant in our analysis.

¹Precise calculations of M_h go beyond the FD approach described here [34]. However, the NHSSM corrections that are the focus of this article are obtained at the one-loop level. Since we are interested only in their relative effects, the restriction to the one-loop corrections in the FD approach is sufficient.

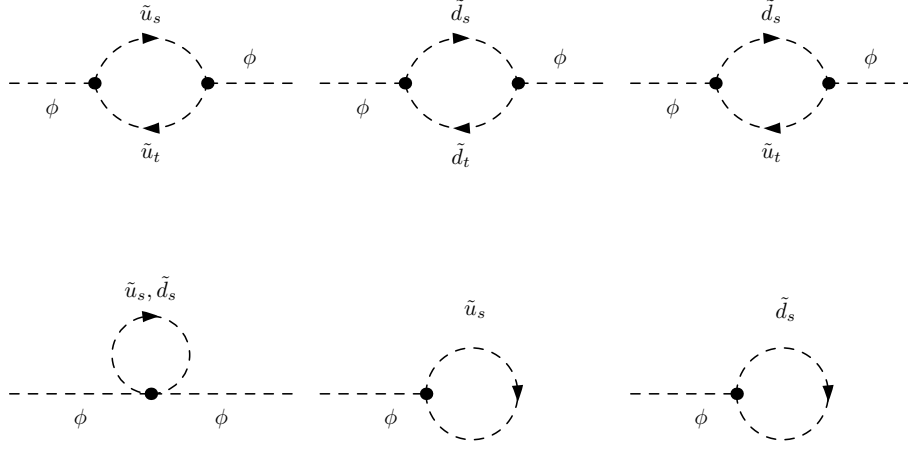


Figure 1: Generic Feynman diagrams for the Higgs boson self-energies and tadpoles. ϕ denotes any of the Higgs bosons, h , H , A or H^\pm ; u stand for u, c, t ; d stand for d, s, b ; $\tilde{u}_{s,t}$ and $\tilde{d}_{s,t}$ are the six mass eigenstates of up-type and down-type squarks, respectively.

3.2 Constraints

In general, the contributions of $T_{33}^{'D}$ to the Higgs masses are anticipated to be large due to the multiplication of the $T_{33}^{'D}$ coupling by $\tan\beta$. In our specific setup, where we maintain the same physical mass spectrum, the value of $T_{33}^{'D}$ could potentially become quite large due to the fixed nature of left-right mixing parameter of the scalar bottom quark X_b (see below for an exact definition). This large $T_{33}^{'D}$ value may result in the violations of constraints related to charge and color breaking minima (CCB). The CCB constraints in the framework of NHSSM were analyzed in Refs. [13, 42] and are given as

$$\left(\sum_{i=d,s,b} (T_{ii} - \mu y_{ii} - T'_{ii}) \right)^2 < \left(\frac{g_1^2 + g_2^2}{2} + 5 \sum_i y_{ii}^2 \right) \times \left(\frac{1}{2} \sum_i (M_{Q_{ii}}^2 + M_{D_{ii}}^2) + m_{H_u}^2 + m_{H_d}^2 + 2|\mu|^2 - 2B_\mu \right). \quad (14)$$

Here, $M_{Q_{ii}}^2$ and $M_{D_{ii}}^2$ denote the soft mass-squared terms for the left-handed squark doublets and right-handed down-type squarks of the i th generation, respectively. The bilinear soft term in the Higgs potential, B_μ , is given by

$$B_\mu = \frac{M_A^2 \sin 2\beta}{2}, \quad (15)$$

while the up- and down-type Higgs boson mass parameters, $m_{H_u}^2$ and $m_{H_d}^2$, are calculated as

$$m_{H_u}^2 = \frac{M_A^2 \cos^2 \beta + \frac{1}{2} M_Z^2 \cos 2\beta - \mu^2}{1 + \tan^2 \beta}, \quad (16)$$

$$m_{H_d}^2 = \frac{M_A^2 \sin^2 \beta - \frac{1}{2} M_Z^2 \cos 2\beta - \mu^2}{1 + \cot^2 \beta}, \quad (17)$$

where M_A is the pseudoscalar Higgs mass, and g_1 and g_2 are the gauge couplings of the $U(1)$ and $SU(2)$ gauge groups, respectively. For our numerical analysis, we wrote a private code based on Eq. (14) to calculate the CCB constraints.

3.3 Computational workflow

To calculate the NH contributions to the Higgs boson masses, we start by generating the NHSSM source code for **SPheno** [27] using the **SARAH** package [28–32]. **SARAH** is a Mathematica-based tool that automates the generation of source code for various new physics models, including the NHSSM. By using the NHSSM model file defined in **SARAH**, we produce the required code, which is then used to calculate the SUSY spectrum including Higgs boson masses, and other relevant observables. For the numerical analysis, we utilize an additional tool, **SARAH Scan and Plot (SSP)** [43], where we define the input parameters. **SSP** generates an SLHA file to be used by **SPheno**, which is then called to calculate the particle spectrum and other observables. The output from **SPheno** is read by **SSP**, which subsequently uses this data for plotting and further analysis.

3.3.1 $T_{33}^{'D}$ analysis

To extract pure $T_{33}^{'D}$ term contributions, it is important that the physical masses and mixing of the scalar bottom remain the same. This can be achieved by fixing the left-right mixing parameter X_b . Consequently, for our numerical evaluation we fix X_b and calculate the value of $T_{33}^{'D}$ for the given value of $T_{33}^{'D}$ using the expression

$$X_b = T_{33}^D - (\mu Y_{33}^D + T_{33}^{'D}) \tan \beta, \quad (18)$$

where $T_{33}^{'D}$ is taken as a free parameter in a specific range i.e. $-100 \text{ GeV} < T_{33}^{'D} < 100 \text{ GeV}$. Concerning the numerical evaluation, for a given value of $T_{33}^{'D}$ in the MSSM and $T_{33}^{'D}$ in the NHSSM a new value of $T_{33}^{'D}$ is calculated such that

$$X_b^{\text{MSSM}} = T_{33}^D \text{ MSSM} - \mu Y_{ij}^D \tan \beta \quad (19)$$

and

$$X_b^{\text{NHSSM}} = T_{33}^D \text{ NHSSM} - (\mu Y_{ij}^D + T_{33}^{'D}) \tan \beta \quad (20)$$

are identical (yielding the same values for the sbottom masses and mixings). Using $T_{33}^D \text{ MSSM}$ and $T_{33}^{'D}$ the NH contribution to the Higgs-boson masses are calculated numerically.

3.3.2 μ' analysis

For the μ' contributions, we set all NH trilinear couplings to zero (including $T_{33}^{'D}$) and fix $\mu + \mu'$ to the value of μ specified in the corresponding scenario. We then vary μ' within the range of -2000 GeV to $+2000 \text{ GeV}$. It should be noted that the parameter μ' does not directly appear in the couplings (see Eq. (6) and Eq. (7)); rather, it enters only through the neutralino and chargino mass matrices (see Eq. (4) and Eq. (5)). The observed effects on the Higgs boson masses arise because we impose the condition $\mu + \mu' = \text{constant}$. Varying μ' leads to a corresponding change in μ , which affects not only the couplings of squarks

and sleptons to the Higgs bosons but also the sfermion mass matrices. Hence, the effects originate from the variation in μ .

Contrary to the approach adopted for $T_{33}^{\prime D}$ analysis, two approaches are followed for the μ' analysis. In the first approach, the holomorphic trilinear terms T_{ii}^f are kept constant, so any change in μ leads to a corresponding change in X_f . As a result, both the Higgs-sfermion couplings and the sfermion masses and mixing are affected, leading to large contributions.

In contrast, in the second approach, X_f is kept fixed, and the change in μ is compensated by an appropriate adjustment of the holomorphic trilinear terms T_{ii}^f . In this case, the contributions arise solely from the variation in μ within the Higgs-sfermion couplings, resulting in smaller contributions.

In the benchmark scenarios used for our analysis (defined in the following section), the holomorphic trilinear couplings are taken to be equal, i.e., $A_t = A_b = A_\tau$. For each point P1–P4 (defined in the next section), these terms are determined from the corresponding value of X_t in that scenario. Using the relation

$$X_t = A_t - \frac{\mu}{\tan \beta}, \quad (21)$$

we compute the holomorphic trilinear couplings $A_t = A_b = A_\tau$, along with the corresponding soft terms T_{33}^U , T_{33}^D , and T_{33}^E . In the first approach, these values are fixed, while X_t , X_b and X_τ vary with changing μ' . In the second approach, X_t , X_b , and X_τ are initially determined for $\mu' = 0$ based on the corresponding values of T_{33}^U , T_{33}^D , and T_{33}^E at that point. Subsequently, X_t , X_b , and X_τ are kept constant by adjusting T_{33}^U , T_{33}^D , and T_{33}^E as μ' varies.

4 Numerical Results

4.1 Input parameters

For our numerical analysis, we opted for three scenarios initially introduced in Ref. [44]. These scenarios, denoted as M_h^{125} , $M_h^{125}(\tilde{\tau})$, and $M_h^{125}(\tilde{\chi})$, provide insight into different aspects of Higgs boson phenomenology within the MSSM. They are characterized by specific SSB parameters and exhibit good agreement with experimental data from the LHC. Each scenario features a \mathcal{CP} -even scalar with a mass approximately around 125 GeV, resembling the SM Higgs boson. In these scenarios, the SSB mass $M_{\tilde{f}}$ for the first two generations is taken as 2 TeV, while the holomorphic trilinear SSB terms for these generations are set to zero. The remaining input parameters are provided in Tab. 1 [44].

In Table 1, $m_{\tilde{Q}_3}$, $m_{\tilde{U}_3}$, and $m_{\tilde{D}_3}$ correspond to the masses of the third generation squark doublet, up-type squark singlet, and down-type squark singlet, respectively. Furthermore, $m_{\tilde{L}_3}$ and $m_{\tilde{E}_3}$ denote the masses of the third generation left-handed slepton doublet and right-handed slepton singlet, respectively. The parameters M_1 , M_2 , and M_3 denote the gaugino masses, while μ represents the standard Higgs mixing parameter. Here, A_τ represent the holomorphic trilinear coupling such that $A_\tau = T_{33}^E/Y_{33}^E$. In these scenarios, the holomorphic trilinear couplings of the third generation are set equal, i.e., $A_t = A_b = A_\tau$, where $A_t = T_{33}^U/Y_{33}^U$ and $A_b = T_{33}^D/Y_{33}^D$, except in the $M_h^{125}(\tilde{\tau})$ scenario, where $A_\tau = 800$ GeV. For each scenario, we investigate four different combinations of M_A and $\tan \beta$, taking into account

	M_h^{125}	$M_h^{125}(\tilde{\tau})$	$M_h^{125}(\tilde{\chi})$
$m_{\tilde{Q}_3}, m_{\tilde{U}_3}, m_{\tilde{D}_3}$	1500	1500	1500
$m_{\tilde{L}_3}, m_{\tilde{E}_3}$	2000	350	2000
μ	1000	1000	180
M_1	1000	180	160
M_2	1000	300	180
M_3	2500	2500	2500
X_t	2800	2800	2500
A_τ	A_t	800	A_t
$m_{\tilde{b}_1}, m_{\tilde{b}_2}$	1339,1662	1339,1662	1358,1646

Table 1: Selected scenarios in the MSSM parameter space, taken from Ref. [44]. All the dimensionful quantities are in GeV.

the latest experimental limits for MSSM Higgs-boson searches [45, 46]:

$$\begin{aligned}
\text{P1 : } & M_A = 1500 \text{ GeV, } \tan \beta = 7 \\
\text{P2 : } & M_A = 2000 \text{ GeV, } \tan \beta = 15 \\
\text{P3 : } & M_A = 2500 \text{ GeV, } \tan \beta = 30 \\
\text{P4 : } & M_A = 2500 \text{ GeV, } \tan \beta = 45
\end{aligned}$$

and define

$$\begin{aligned}
\delta M_h &\equiv M_h^{\text{NHSSM}} - M_h^{\text{MSSM}}, \\
\delta M_H &\equiv M_H^{\text{NHSSM}} - M_H^{\text{MSSM}}, \\
\delta M_{H^\pm} &\equiv M_{H^\pm}^{\text{NHSSM}} - M_{H^\pm}^{\text{MSSM}}.
\end{aligned} \tag{22}$$

Here $M_{h,H,H^\pm}^{\text{MSSM}}$ represents the values of M_{h,H,H^\pm} when NH terms $T_{33}^{\prime D}$ and μ' are set to zero.

4.2 NH contributions to the Higgs-boson masses

4.2.1 μ' contributions

In this section, we present our results for μ' contributions to Higgs boson masses. As already explained, we fix $\mu + \mu'$ to the value of μ in the respective scenario. This approach will keep the chargino and neutralino phenomenology (masses and mixing) unchanged which will have important consequences for the dark matter relic abundance. For example, we have verified that $\Omega_{\text{CDM}} h^2$ remains unchanged for all points in the M_h^{125} and $M_h^{125}(\tilde{\chi})$ scenarios. However, it varies in the $M_h^{125}(\tilde{\tau})$ scenario. In this case, the charged slepton, i.e., \tilde{e}_1 , becomes the next-to-lightest supersymmetric particle (NLSP), and the change arises due to variations in the masses $m_{\tilde{e}_{1,2}}$. These mass variations result from changes in μ , as there is no compensating factor μ' in the scalar lepton mass matrix. On the other hand, in the original definition of the benchmark planes in Ref. [44], DM was *not* considered as a relevant constraint. The reason is that the parameters affecting the DM relic density have only a small impact on the Higgs-boson sector. Furthermore, a small amount of R-parity violation would fully invalidate any bounds on the DM relic density, while having a negligible impact on the Higgs-sector phenomenology.

Furthermore, it is important to note that point P1 is ruled out by CCB constraints, as the small value of M_A at this point causes the left-hand side of Eq. (14) to dominate. Nevertheless, we show the contributions from P1 for completeness. Also here it should be noted that these constraints were not considered in the original definition of the benchmark planes in Ref. [44].

In Fig. 2, we present our results for the contributions of μ' to M_h in the M_h^{125} (upper row), $M_h^{125}(\tilde{\chi})$ (middle row), and $M_h^{125}(\tilde{\tau})$ (lower row) scenarios. In the left panel, we show the result where T_{ii}^f are fixed whereas right panel show the results where X_f is fixed. For cases where the holomorphic trilinear terms T_{ii}^f are fixed, the largest contributions occur at lower values of M_A and $\tan\beta$ in M_h^{125} . Specifically, at point P1, the contributions can reach up to +350 MeV and -850 MeV, while other points exhibit comparatively smaller contributions. In the $M_h^{125}(\tilde{\chi})$ scenario, point P1 contributions can reach up to +150 MeV and -650 MeV, whereas contributions from other points remain below 200 MeV except for the point P4 which can reach up to -1 GeV for large values of μ' . In contrast, the $M_h^{125}(\tilde{\tau})$ scenario exhibits a different trend, with the largest contributions arising from point P4, reaching up to -15 GeV, while point P3 contributes up to -13 GeV. For point P4 (P3), values of $\mu' < -400$ (-1200) GeV are not allowed, as they lead to negative slepton squared masses. The apparently large contributions arise from the fixed value of the holomorphic trilinear term A_τ in this scenario. Moreover, due to the small values of $m_{\tilde{L}_3}, m_{\tilde{E}_3}$, the masses of the scalar taus are significantly affected by changes in μ , leading to large contributions. Thus, the large effects should be viewed more as an artifact of the definition of the benchmark scenario. Previously, we emphasized that pure NHSSM contributions can only be isolated if the masses and mixing angles are held constant. However, in the current approach—where we fix T_{ii}^f to a constant value while allowing X_f to vary—the physical mass spectrum of the sfermions is affected. Although the spectrum changes, we have explicitly verified that the variations remain within 2% in most cases, which is well below the expected experimental uncertainty. An exception arises in the $M_h^{125}(\tilde{\tau})$ scenario, where the variation in slepton masses can be significant. This behavior, however, should be attributed to the specific structure of the scenario, as discussed above.

For cases where X_f is fixed, the contributions remain small. In the M_h^{125} scenario, point P4 exhibits the largest contributions, reaching up to ± 45 MeV. Similarly, in the $M_h^{125}(\tilde{\chi})$ scenario, P4 again shows the largest contributions, reaching up to -1.4 GeV, while other points showing only minor contributions.

In the $M_h^{125}(\tilde{\tau})$ scenario, although the left-right mixing parameters for scalar top and scalar bottom quarks are fixed, the trilinear holomorphic term T_{33}^E is also fixed due to the scenario definition. Consequently, the left-right mixing parameter for scalar tau lepton varies, leading to contributions similar to those observed when X_f was not fixed.

In Fig. 3, we present our results for δM_H as a function of μ' . The plot arrangement follows the same structure as in the previous figure. For the case where the holomorphic trilinear terms T_{ii}^f are fixed (left panel), the largest contributions occur at point P4, reaching up to +44 GeV and -26 GeV in the M_h^{125} scenario, and up to +20 GeV and -40 GeV in the $M_h^{125}(\tilde{\chi})$ scenario. In $M_h^{125}(\tilde{\tau})$ scenario, the largest contributions are again for P4 where they reach up to +44 GeV. However, for negative values of μ' , the contributions from P2 can reach up to -20 GeV. For the case where X_f is fixed (right panel), the overall trend remains the same, though the contributions in some cases are slightly different compared to

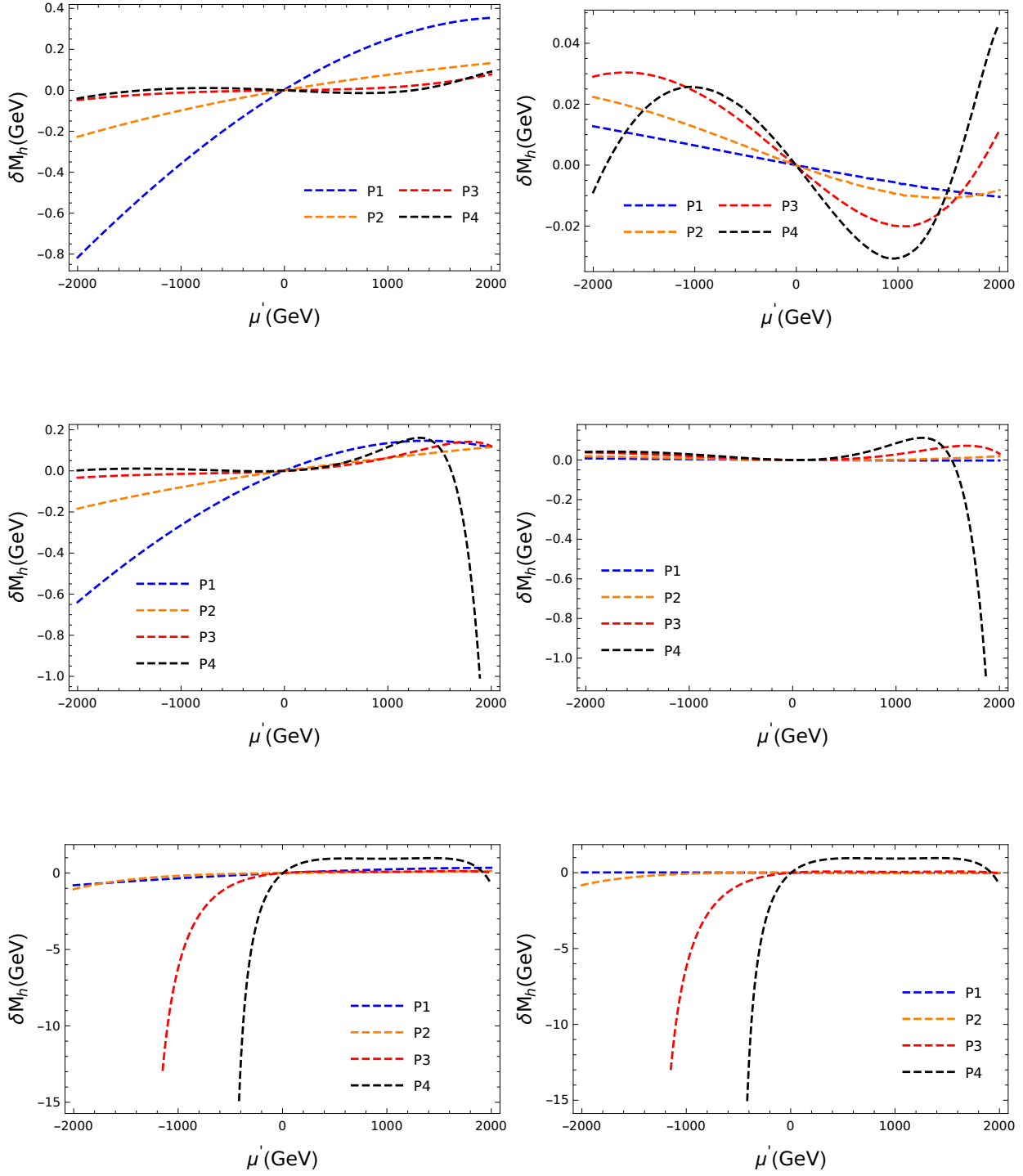


Figure 2: δM_h as a function of μ' for M_h^{125} (upper row), $M_h^{125}(\tilde{\chi})$ (middle row) and $M_h^{125}(\tilde{\tau})$ (lower row) scenarios for fixed T_{ii}^f (left panel) and fixed X_f (right panel).

those in the fixed T_{ii}^f scenario.

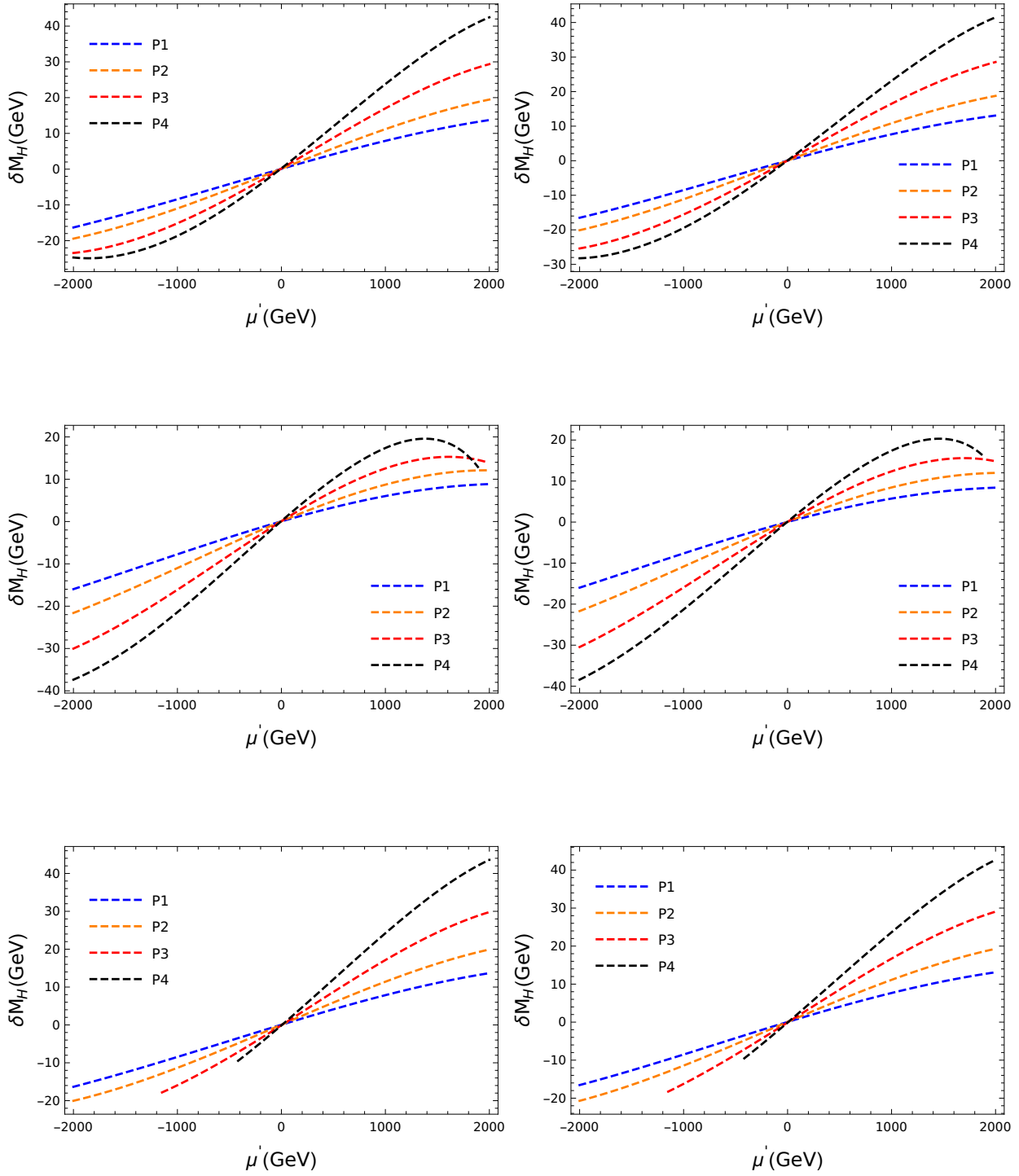


Figure 3: δM_H as a function of μ' for M_h^{125} (upper row), $M_h^{125}(\tilde{\chi})$ (middle row) and $M_h^{125}(\tilde{\tau})$ (lower row) scenarios for fixed T_{ii}^f (left panel) and fixed X_f (right panel).

In Fig. 4, we show our results for $\delta M_{H\pm}$ as a function of μ' , with the plot arrangement consistent with the previous figures. In the M_h^{125} scenario with fixed T_{ii}^f (left panel), point P4 exhibits the most significant negative contribution, reaching up to -22 GeV, while small positive contributions of up to $+2$ GeV are also observed for this point. Contributions from other points remain within ± 10 GeV or lower. Similarly, in the $M_h^{125}(\tilde{\chi})$ scenario, P4 again shows the largest contributions, reaching up to $+7$ GeV and -44 GeV. The $M_h^{125}(\tilde{\tau})$ scenario exhibits the most pronounced effects, with point P4 contributing up to -18 GeV. For the fixed X_f scenario, the contributions are generally 2 to 3 GeV smaller than those observed in the fixed T_{ii}^f case.

4.2.2 $T_{33}'^D$ contributions

In this section, we present our findings regarding the impact of $T_{33}'^D$ on the Higgs-boson masses M_h , M_H , and $M_{H\pm}$. As previously discussed, in these scenarios, the holomorphic trilinear couplings are equal by definition, i.e., $A_t = A_b$. These couplings, along with the corresponding T_{33}^U and T_{33}^D , can be determined from the value of X_t . In Tab. 2, we show the values of the holomorphic trilinear coupling T_{33}^D for the benchmark points P1 to P4 in the M_h^{125} and $M_h^{125}(\tilde{\chi})$ scenarios. These values correspond to three choices of $T_{33}'^D$: -100 GeV (Min), 0 (Central), and 100 GeV (Max). Since the input parameters μ and X_t are identical in the M_h^{125} and $M_h^{125}(\tilde{\tau})$ scenarios, the results for the latter are the same as those in the M_h^{125} case and are not shown separately.

	M_h^{125}			$M_h^{125}(\tilde{\chi})$		
Point	Min	Central	Max	Min	Central	Max
P1	-650	50	750	-747	-48	652
P2	-1451	48	1549	-1660	-160	1340
P3	-2951	48	3048	-3370	-370	2630
P4	-4452	48	4547	-5080	-579	3920

Table 2: Values of T_{33}^D (in GeV) for points P1–P4 in the M_h^{125} and $M_h^{125}(\tilde{\chi})$ scenarios, corresponding to $T_{33}'^D = -100$ GeV (Min), $T_{33}'^D = 0$ (Central), and $T_{33}'^D = 100$ GeV (Max). The values for the $M_h^{125}(\tilde{\tau})$ scenario are identical to those of the M_h^{125} scenario, as the input parameters μ and X_t are the same in both cases.

For our numerical evaluation, we vary $T_{33}'^D$ in the range of -100 GeV to 100 GeV. In principle, the $T_{33}'^D$ contributions can be substantial due to the multiplication of the $T_{33}'^D$ term by $\tan\beta$. The plots in Fig. 5 illustrates the value of δM_h as a function of $T_{33}'^D$. The left plot corresponds to the M_h^{125} scenario, while the right plot shows the results in the $M_h^{125}(\tilde{\chi})$ scenario. Since the input parameters for the scalar quark sector are the same in M_h^{125} and $M_h^{125}(\tilde{\tau})$, the results for $M_h^{125}(\tilde{\tau})$ align with those of M_h^{125} and are therefore not displayed separately. As anticipated, the most notable effects occur in the P4, characterized by the highest $\tan\beta$ value. For this point, the modifications can be as large as 75 MeV for the M_h^{125} scenario and up to 90 MeV for the $M_h^{125}(\tilde{\chi})$ scenario.

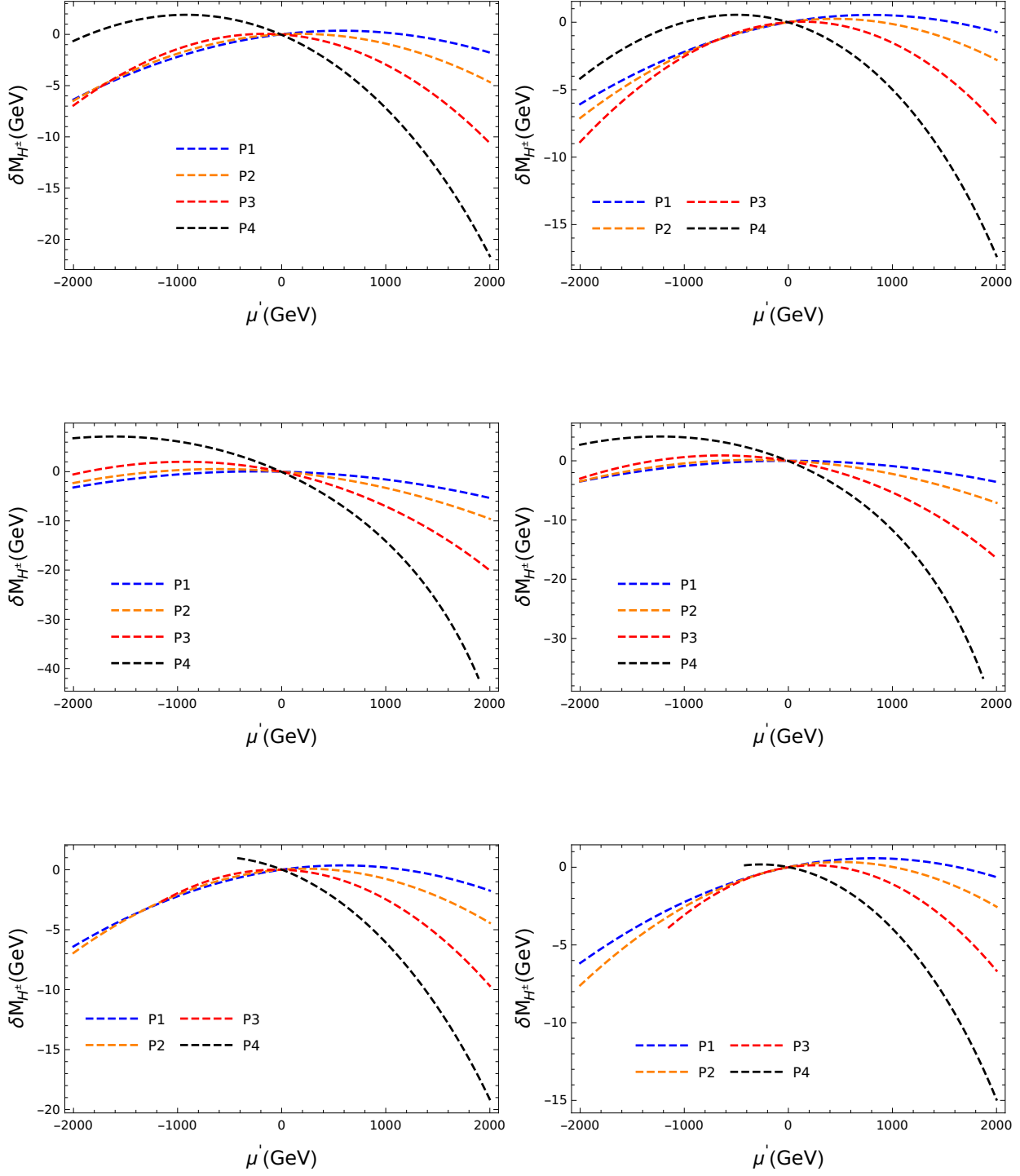


Figure 4: δM_{H^\pm} as a function of μ' for M_h^{125} (upper row), $M_h^{125}(\tilde{\chi})$ (middle row) and $M_h^{125}(\tilde{\tau})$ (lower row) scenarios for fixed T_{ii}^f (left panel) and fixed X_f (right panel).

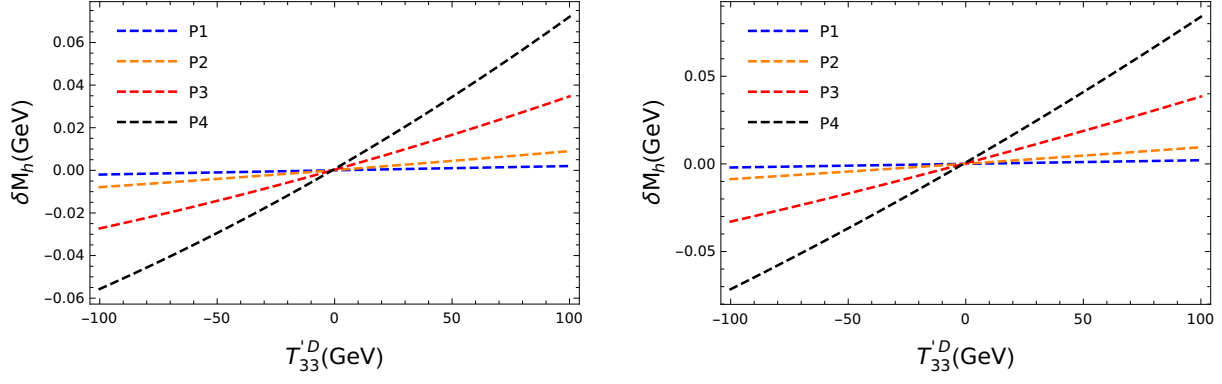


Figure 5: δM_h as a function of T'_{33} for M_h^{125} (left plot) and $M_h^{125}(\tilde{\chi})$ (right plot).

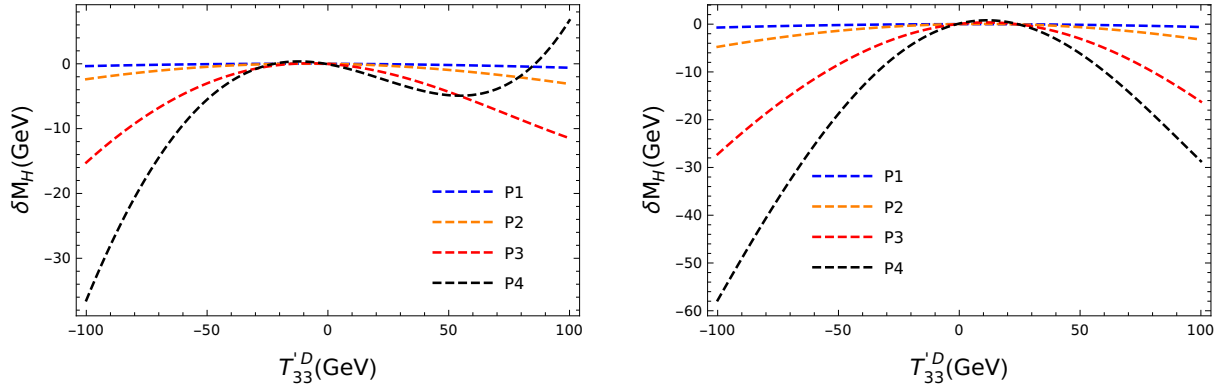


Figure 6: δM_H as a function of T'_{33} for M_h^{125} (left plot) and $M_h^{125}(\tilde{\chi})$ (right plot).

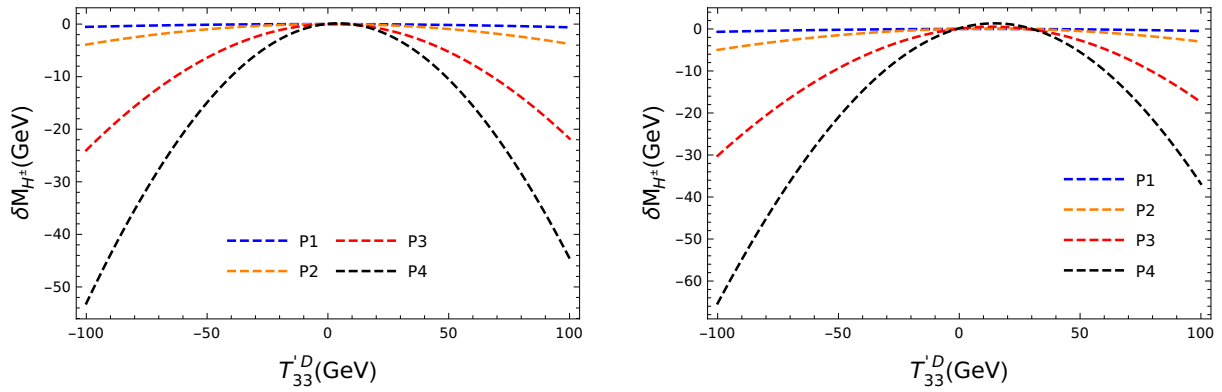


Figure 7: δM_{H^\pm} as a function of T'_{33} for M_h^{125} (left plot) and $M_h^{125}(\tilde{\chi})$ (right plot).

In Figure 6, we depict δM_H as a function of $T_{33}^{'D}$. The layout of plots is the same as in Fig. 5. In the context of the M_h^{125} scenario, the most substantial contributions are observed for the point P3 and P4, yielding negative contributions of up to 16 GeV, however, P4 can result in negative contribution of up to 38 GeV. On the other hand, in the $M_h^{125}(\tilde{\chi})$ scenario, the most significant impact emerges from the point P4, resulting in a negative contribution of up to 58 GeV.

Finally, our findings for δM_{H^\pm} as a function of $T_{33}^{'D}$ are presented in Figure 7. The arrangement of plots follows the same pattern as the previous figures. Once again, the most substantial contributions are associated with the point P4. In the M_h^{125} and $M_h^{125}(\tilde{\chi})$ scenarios, these contributions can extend up to 54 GeV and 66 GeV respectively.

It should be noted that if the effects arise through mass matrices, then for $T_{33}^{'D}$, one would expect significant effects on M_h due to the multiplication of the $T_{33}^{'D}$ term by $\tan \beta$ in the mass matrix. However, in our approach, where the mass spectrum is fixed by keeping X_b constant, the situation is reversed. In this case, the multiplication of $T_{33}^{'D}$ by $\tan \beta$ causes T_{33}^D to become very large. Since this term is multiplied by c_α in the couplings of the \mathcal{CP} -even heavy Higgs H , the dominant contributions appear in M_H .

5 Conclusions

In this paper, we have investigated the effect of non-holomorphic (NH) soft SUSY-breaking terms to the Higgs-boson mass predictions in the NHSSM. In a previous paper [26] we concentrated on the effect of the NH trilinear Higgs-scalar top coupling, $T_{33}^{'U}$. In this paper we complement that work with an analysis of the NH trilinear Higgs-scalar bottom coupling, $T_{33}^{'D}$ and the NH higgsino mass parameter, μ' . In order to perform the calculations, using the Mathematica package **SARAH**, we generated a **Spheno** version including the NH contributions to the Higgs-boson self-energies. This **Spheno** version was then employed for the numerical analysis.

We took particular care to analyze the pure NH contribution. The NH SSB terms enter into the respective mass matrices, in this case the scalar bottom and the chargino/neutralino mass matrices. The $T_{33}^{'D}$ term modifies both the scalar bottom mass matrix and the Higgs-scalar bottom couplings. In contrast, μ' appears only in the chargino and neutralino mass matrices, but not in the couplings between the Higgs bosons and the charginos/neutralinos. An analysis simply varying the NH SSB terms thus leads to a shift in the scalar bottom and/or chargino/neutralino masses, which should be considered as a different physics scenario, as it is expected that the masses and mixing angles of the contributing SUSY particles are measured in the future (if SUSY is realized). Consequently, an observed effect from a naive variation of the NH SSB terms can be mimicked by a change in the holomorphic SSB terms. Concretely, for each choice of $T_{33}^{'D}$ the parameter T_{33}^D can be adjusted to yield the same scalar bottom masses. An observed sbottom mass spectrum thus corresponds to a continuous set of combinations of T_{33}^D and $T_{33}^{'D}$ (keeping the other SSB and μ fixed). An analysis that simply varies $T_{33}^{'D}$, resulting in shifts in the sbottom masses and mixings, can thus not be regarded realistic. Therefore, in our analysis, we required X_b to be constant under a change of $T_{33}^{'D}$ by an adjustment of T_{33}^D . In this way, the effect of the NH contributions is shifted into the Higgs-sbottom couplings and can readily be analyzed. A similar strategy has been followed for

μ' , where we required that $\mu' + \mu$, as they appear in the chargino/neutralino mass matrices, remains constant. However, here another subtlety arises, as μ , but not μ' , also enters into the scalar fermion mass matrices. Here we used two different options. In the first approach, the holomorphic trilinear terms are fixed according to the values defined in the respective scenarios. Consequently, variations in μ' , and thereby in μ , lead to changes in the left-right mixing parameters X_f . Although the masses and mixing angles in this case change, we have explicitly verified that the resulting shifts remain below 2% in the majority of cases, staying well within the anticipated experimental uncertainty. In the second approach, however, the change in μ' is compensated by a corresponding adjustment in the holomorphic trilinear terms, keeping X_f constant.

For the numerical analysis, we chose three LHC benchmark scenarios (M_h^{125} , $M_h^{125}(\tilde{\tau})$ and $M_h^{125}(\tilde{\chi})$) [44]. In each scenario, four combinations of $(M_A, \tan\beta)$ were chosen that are allowed by current MSSM Higgs-boson searches at the LHC, (1000 GeV, 7), (1500 GeV, 15), (2500 GeV, 30), (2500 GeV, 45), called P1, P2, P3, P4, respectively. $T_{33}'^D$ has been varied from -100 GeV to $+100$ GeV, whereas μ' was varied from -2000 GeV to $+2000$ GeV. The relatively small range for $T_{33}'^D$ was chosen to avoid too large effects in T_{33}^D .

Concerning the numerical analysis of a variation of $T_{33}'^D$, the results in the M_h^{125} and the $M_h^{125}(\tilde{\tau})$ scenario, are effectively identical due to their identical settings in the scalar quark sector. The results in the $M_h^{125}(\tilde{\chi})$ scenario, however, can vary visibly from the other two scenarios. For δM_h the NH contributions yield corrections that are in general found to be very small, and at a similar level of the $T_{33}'^U$ variation [26] (but contrary to previous claims in the literature). They reach up to $\sim \pm 60$ MeV in the analyzed parameter space, where P4 exhibits the largest corrections. Since the corrections turn out to be very small over the whole analyzed parameter space we find that the NH terms *do not* alleviate the fact that large SUSY masses are needed to reach the value of $M_h \sim 125$ GeV. The numerical effects for M_H and $M_{H\pm}$ were found to be mostly negative and reached values of up to ~ -60 GeV for M_H and $M_{H\pm}$.

Concerning the analysis of a variation of μ' , the size of the numerical effects depend on the choice of the adjustment of the holomorphic SSB terms. They can go down to $\delta M_h \sim -1$ GeV in the M_h^{125} and $M_h^{125}(\tilde{\chi})$ scenarios, and due to a specific definition of the scalar lepton sector down to ~ -15 GeV in the $M_h^{125}(\tilde{\tau})$ scenario. However, those parameter points would then yield a light \mathcal{CP} -even Higgs-boson mass well below 125 GeV, i.e. they would be experimentally excluded. The numerical effects on M_H range roughly between -40 GeV and $+40$ GeV, while the effects on $M_{H\pm}$ are mostly negative, going down to ~ -20 GeV in the M_h^{125} and the $M_h^{125}(\tilde{\tau})$ scenario, and down to ~ -40 GeV in the $M_h^{125}(\tilde{\chi})$ scenario.

Despite the fact that the NH contributions entering via $T_{33}'^D$ and μ' are mostly small for M_h (the same holds for $T_{33}'^U$), a full analysis of supersymmetric extensions of the SM should include the possibility of NH contributions. Consequently, we aim for an inclusion of these effects into the code **FeynHiggs** [47–54], thus providing the NHSSM mass spectrum with the highest possible precision.

Acknowledgments

S.H. acknowledges partial financial support by the Spanish Research Agency (Agencia Estatal de Investigación) through the grant IFT Centro de Excelencia Severo Ochoa No CEX2020-001007-S funded by MCIN/AEI/10.13039/501100011033. The work of S.H. was also supported by the Grant PID2022-142545NB-C21 funded by MCIN/AEI/10.13039/501100011033/FEDER, UE.

References

- [1] P. Fayet, Nucl. Phys. B **90** (1975), 104-124
- [2] P. Fayet, Phys. Lett. B **64** (1976), 159
- [3] P. Fayet, Phys. Lett. B **69** (1977), 489
- [4] H. P. Nilles, Phys. Rept. **110** (1984), 1-162
- [5] H. E. Haber and G. L. Kane, Phys. Rept. **117** (1985), 75-263
- [6] R. Barbieri, Riv. Nuovo Cim. **11N4** (1988), 1-45
- [7] S. Sekmen [ATLAS, CMS and LHCb], [arXiv:2204.03053 [hep-ex]].
- [8] L. Girardello and M. T. Grisaru, Nucl. Phys. B **194** (1982), 65
- [9] J. Bagger and E. Poppitz, Phys. Rev. Lett. **71** (1993), 2380-2382 [arXiv:hep-ph/9307317 [hep-ph]].
- [10] U. Chattopadhyay, D. Das and S. Mukherjee, JHEP **01** (2018), 158 [arXiv:1710.10120 [hep-ph]].
- [11] C. S. Un, Turk. J. Phys. **48** (2024) no.1, 1-27 [arXiv:2308.12862 [hep-ph]].
- [12] U. Chattopadhyay, A. Datta, S. Mukherjee and A. K. Swain, JHEP **10** (2018), 202 [arXiv:1809.05438 [hep-ph]].
- [13] U. Chattopadhyay, D. Das and S. Mukherjee, JHEP **06** (2020), 015 [arXiv:1911.05543 [hep-ph]].
- [14] U. Chattopadhyay, A. Datta, S. Mukherjee and A. K. Swain, JHEP **08** (2022), 113 [arXiv:2201.00621 [hep-ph]].
- [15] J. Chakraborty and S. Roy, Phys. Rev. D **85** (2012), 035014 [arXiv:1104.1387 [hep-ph]].
- [16] S. Israr and M. Rehman, [arXiv:2407.01210 [hep-ph]].
- [17] M. Rehman and S. Heinemeyer, [arXiv:2411.00479 [hep-ph]].
- [18] S. Israr, M. E. Gómez and M. Rehman, Particles **8** (2025) no.1, 30
- [19] I. Jack and D. Jones, Phys. Lett. B **457** (1999), 101-108 [arXiv:hep-ph/9903365 [hep-ph]].
- [20] I. Jack and D. Jones, Phys. Rev. D **61** (2000), 095002 [arXiv:hep-ph/9909570 [hep-ph]].
- [21] I. Jack, D. Jones and A. Kord, Phys. Lett. B **588** (2004), 127-135 [arXiv:hep-ph/0402045 [hep-ph]].

- [22] M. Cakir, S. Mutlu and L. Solmaz, Phys. Rev. D **71** (2005), 115005 [arXiv:hep-ph/0501286 [hep-ph]].
- [23] A. Sabanci, A. Hayreter and L. Solmaz, Phys. Lett. B **661** (2008), 154-157 [arXiv:0801.2029 [hep-ph]].
- [24] C. S. Un, S. H. Tanyıldızı, S. Kerman and L. Solmaz, Phys. Rev. D **91** (2015) no.10, 105033 [arXiv:1412.1440 [hep-ph]].
- [25] U. Chattopadhyay and A. Dey, JHEP **1610**, 027 (2016)
- [26] M. Rehman and S. Heinemeyer, Phys. Rev. D **107** (2023) no.9, 095033 [arXiv:2212.13757 [hep-ph]].
- [27] W. Porod, Comput. Phys. Commun. **153** (2003), 275-315 [arXiv:hep-ph/0301101 [hep-ph]].
- [28] F. Staub, Comput. Phys. Commun. **181** (2010), 1077-1086 [arXiv:0909.2863 [hep-ph]].
- [29] F. Staub, Comput. Phys. Commun. **182** (2011), 808-833 [arXiv:1002.0840 [hep-ph]].
- [30] F. Staub, Comput. Phys. Commun. **184** (2013), 1792-1809 [arXiv:1207.0906 [hep-ph]].
- [31] F. Staub, Comput. Phys. Commun. **185**, 1773 (2014) [arXiv:1309.7223 [hep-ph]].
- [32] F. Staub, Adv. High Energy Phys. **2015** (2015), 840780 [arXiv:1503.04200 [hep-ph]].
- [33] P. Draper and H. Rzehak, Phys. Rept. **619**, 1-24 (2016) [arXiv:1601.01890 [hep-ph]].
- [34] P. Slavich and S. Heinemeyer (eds), E. Bagnaschi, H. Bahl, M. Goodsell, H. E. Haber, T. Hahn, R. Harlander, W. Hollik and G. Lee, *et al.* Eur. Phys. J. C **81** (2021) no.5, 450 [arXiv:2012.15629 [hep-ph]].
- [35] S. Heinemeyer, O. Stal and G. Weiglein, Phys. Lett. B **710** (2012), 201-206 [arXiv:1112.3026 [hep-ph]].
- [36] S. Navas *et al.* [Particle Data Group], Phys. Rev. D **110** (2024) no.3, 030001
- [37] M. Cepeda, S. Gori, P. Ilten, M. Kado, F. Riva, R. Abdul Khalek, A. Aboubrahim, J. Alimena, S. Alioli and A. Alves, *et al.* CERN Yellow Rep. Monogr. **7** (2019), 221-584 [arXiv:1902.00134 [hep-ph]].
- [38] P. Bambade, T. Barklow, T. Behnke, M. Berggren, J. Brau, P. Burrows, D. Denisov, A. Faus-Golfe, B. Foster and K. Fujii, *et al.* [arXiv:1903.01629 [hep-ex]].
- [39] J. de Blas, M. Cepeda, J. D'Hondt, R. K. Ellis, C. Grojean, B. Heinemann, F. Maltoni, A. Nisati, E. Petit and R. Rattazzi, *et al.* JHEP **01** (2020), 139 [arXiv:1905.03764 [hep-ph]].
- [40] S. Gennai, S. Heinemeyer, A. Kalinowski, R. Kinnunen, S. Lehti, A. Nikitenko and G. Weiglein, Eur. Phys. J. C **52** (2007), 383-395 [arXiv:0704.0619 [hep-ph]].

- [41] M. Frank, L. Galeta, T. Hahn, S. Heinemeyer, W. Hollik, H. Rzehak and G. Weiglein, *Phys. Rev. D* **88** (2013) no.5, 055013 [arXiv:1306.1156 [hep-ph]].
- [42] J. Beuria and A. Dey, *JHEP* **10** (2017), 154 [arXiv:1708.08361 [hep-ph]].
- [43] F. Staub, T. Ohl, W. Porod and C. Speckner, *Comput. Phys. Commun.* **183** (2012), 2165-2206 [arXiv:1109.5147 [hep-ph]].
- [44] E. Bagnaschi, H. Bahl, E. Fuchs, T. Hahn, S. Heinemeyer, S. Liebler, S. Patel, P. Slavich, T. Stefaniak, C. E. Wagner and G. Weiglein, *Eur. Phys. J. C* **79** (2019) no.7, 617 [arXiv:1808.07542 [hep-ph]].
- [45] G. Aad *et al.* [ATLAS], *Phys. Rev. Lett.* **125** (2020) no.5, 051801 [arXiv:2002.12223 [hep-ex]].
- [46] [CMS], [arXiv:2208.02717 [hep-ex]].
- [47] S. Heinemeyer, W. Hollik and G. Weiglein, *Eur. Phys. J. C* **9** (1999) 343 [arXiv:hep-ph/9812472].
- [48] G. Degrandi, S. Heinemeyer, W. Hollik, P. Slavich and G. Weiglein, *Eur. Phys. J. C* **28** (2003) 133 [arXiv:hep-ph/0212020].
- [49] M. Frank, T. Hahn, S. Heinemeyer, W. Hollik, R. Rzehak and G. Weiglein, *JHEP* **0702** (2007) 047 [arXiv:hep-ph/0611326].
- [50] M. Frank, T. Hahn, S. Heinemeyer, W. Hollik, H. Rzehak and G. Weiglein, *JHEP* **0702**, 047 (2007) [hep-ph/0611326].
- [51] T. Hahn, S. Heinemeyer, W. Hollik, H. Rzehak and G. Weiglein, *Phys. Rev. Lett.* **112** (2014) 141801 [arXiv:1312.4937 [hep-ph]].
- [52] H. Bahl and W. Hollik, *Eur. Phys. J. C* **76** (2016) no.9, 499 [arXiv:1608.01880 [hep-ph]].
- [53] H. Bahl, S. Heinemeyer, W. Hollik and G. Weiglein, *Eur. Phys. J. C* **78** (2018) no.1, 57 [arXiv:1706.00346 [hep-ph]].
- [54] H. Bahl, T. Hahn, S. Heinemeyer, W. Hollik, S. Paßehr, H. Rzehak and G. Weiglein, *Comput. Phys. Commun.* **249** (2020), 107099 [arXiv:1811.09073 [hep-ph]].